Numerical investigation of non-Newtonian water-CMC/CuO nanofluid flow in an offset strip-fin microchannel heat sink: Thermal performance and thermodynamic considerations

Abdullah A.A.A. Al-Rashed [a], Amin Shahsavar [b, *], Sajad Entezari [b], M.A. Moghimi [c], S.A. Adio [d], Truong Khang Nguyen [e, f, *]

a Department of Automotive and Marine Engineering Technology, College of Technological Studies, The Public Authority for Applied Education and Training, Kuwait
b Department of Mechanical Engineering, Kermanshah University of Technology, Kermanshah, Iran
c Department of Mechanical and Aeronautical Engineering, University of Pretoria, Pretoria, South Africa
d Department of Mechanical Engineering, Obafemi Awolowo University, Ile-Ife, Nigeria
e Division of Computational Physics, Institute for Computational Science, Ton Duc Thang University, Ho Chi Minh City, Viet Nam
f Faculty of Electrical and Electronics Engineering, Ton Duc Thang University, Ho Chi Minh City, Viet Nam

** Corresponding authors at: Division of Computational Physics, Institute for Computational Science, Ton Duc Thang University, Ho Chi Minh City, Viet Nam (T.K. Nguyen). Email addresses: a.shahsavar@kut.ac.ir (A. Shahsavar); tranminhduc@tdtu.edu.vn (T.K. Nguyen)*

Abstract

This paper aims to investigate the hydrothermal and entropy generation characteristics of a non-Newtonian nanofluid containing CuO nanoparticles in an offset strip-fin microchannel heat sink (MCHS). The base fluid is solution of 0.5 wt% Carboxymethyl Cellulose (CMC) in water. This study investigates the effects of nanoparticles concentration, Reynolds number and geometric size of strip-fin on the performance of MCHS from the viewpoint of both the first and the second thermodynamic law. The results reveal that enhancing the Reynolds number improves the performance of MCHS by boosting the convective heat transfer coefficient of the working fluid which favourably reduces the CPU surface temperature and thermal entropy generation rate and importantly leads to the temperature uniformity of the CPU surface. However, increase in Reynolds number adversely affects both the pumping power and the frictional entropy generation in the system. Therefore, the optimal strip-fin size is investigated to find the optimum performance of the offset strip-fins MCHS from the viewpoint of both the first and the second thermodynamic law. The optimal results show that the highest ratio of heat transfer enhancement to pressure drop increment, using the nanofluid instead of base fluid, is 2.29. In addition in the optimal case, the minimum total entropy generation rate of the nanofluid is 2.7% less than the base fluid.

Keywords:
Non-Newtonian Nanofluid; Microchannel heat sink, Entropy generation, Electronics cooling, Thermal performance; Numerical simulation

Nomenclature

$c_{p,nf}$	specific heat capacity (J/kg K)
D_h	hydraulic diameter (m)
H	thickness of the MCHS (m)
H_c	channel height (m)
h	convective heat transfer coefficient (W/m^2 K)
k	thermal conductivity (W/m K)
L	length of the MCHS (m)
L_i	fin interval (m)
L_s	fin length (m)
m	consistency index (kg s^{n-1}/m)
n	power law index
p	pressure (Pa)
P_{pump}	pumping power (W)
Δp	pressure drop (Pa)
PEC	performance evaluation criterion
q''	heat flux (W/m^2)
$\dot{Q}$	volumetric flow rate (m^3/s)
R	thermal resistance (K m^2/W)
Re	Reynolds number
$\dot{S}'''_F$	local frictional entropy generation rate (W/m^3 K)
$\dot{S}'''_H$	local thermal entropy generation rate (W/m^3 K)

$\dot{S}_T'''$	local total entropy generation rate (W/m^3 K)
$\dot{S}_F$	global frictional entropy generation rate (W/K)
$\dot{S}_H$	global thermal entropy generation rate (W/K)
$\dot{S}_T$	global total entropy generation rate (W/K)
T	temperature (K)
T_{nf}^{mean}	mean temperature of nanofluid (K)
T_s^{max}	maximum temperature of the base of the MCHS (K)
T_s^{mean}	mean temperature of the base of the MCHS (K)
T_s^{min}	minimum temperature of the base of the MCHS (K)
u	velocity (m/s)
u_x	x-direction velocity (m/s)
u_y	y-direction velocity (m/s)
u_z	z-direction velocity (m/s)
W	width of the MCHS (m)
W_c	channel thickness (m)
W_w	fin width (m)

Greek symbols

δ	ratio of fin offset to fin length
θ	temperature non-uniformity per unit flux (K m^2/W)
μ	viscosity (kg/m s)
ρ	density (kg/m^3)
φ	nanoparticle concentration (%)
χ	number of fins along the channel length

Subscripts

bf	base fluid
nf	nanofluid
p	particle
s	wall

1. Introduction

The recent technological advancement in the electronics industry with the advent of high energy density devices is accompanied with thermal management challenges. The heat flux in these systems is expected to exceed 100 W/cm^2 and, as such, cooling technologies including MCHS are constantly being improved to take care of the associated thermal challenges. In the last two decades, various approaches have been proposed towards solving the problem of elevated temperature and hotspot situations in many systems including electronic modules (CPU) that are mostly beset with space constraint. Some of these methods include geometric optimisation of heat exchanger, the use of functionally graded materials and the use of a fluid with improved thermal properties including nanofluids as the working fluid. The use of functionally graded materials raises concerns regarding the affordability of the product where these materials are used. However, both geometric optimisation and use of nanofluid have shown considerable significance on an individual basis.

Nanofluids are the new heat transfer fluids formulated by uniform dispersion of ultrafine nanoparticles (1–100 nm) in the conventional heat transfer fluids (base fluids) such as water, glycerol, ethylene glycol and propylene glycol. The research findings in the past couple of decades have revealed that nanofluids have superior thermal and electrical properties [1–7]. These superior properties project nanofluids as potential heat transfer fluids for emergent thermal systems such as nanoelectromechanical systems (NEMs) and microelectromechanical systems (MEMs) and high energy density electronic modules. On this basis, some of the foremost researchers had shown the importance of applying nanoparticles to create nano-refrigerants (refrigerant plus nanoparticles) as working fluid in flow boiling heat transfer in horizontal tubes [8–10], as an automobile radiator fluid [11] and as a working fluid in heat pipe [12–14] heat exchanger.

Numerical simulation of nanofluids in MCHS devices is a relatively new area of application of nanofluids and there are different models that can be applied to solve this thermal-flow problem in order to capture the heat transfer enhancement mechanism. Yue et al [15] applied a single-phase model to numerically investigate the performance of a manifold heat sink with water-Al_2O_3 nanofluid as the heat transfer fluid. They studied the effect of nanoparticle volume fraction and size, and the flow Reynolds number, while the thermal performance was measured by the Nusselt number, pressure drop, total entropy generation, and performance index. Their results showed that the Nusselt number and the pressure drop increased as the nanoparticle volume fraction was increased, while the entropy generation in the system decreased. Conversely, the Nusselt number, the pressure drop and the entropy generation increased with an increase in the particle size, while the performance index reduced. Other research works where single-phase model was used for determining nanofluids thermal performance in a microchannel can be reviewed here [16–18].

As nanofluids consist of two-phase materials (solid + liquid), researchers have also applied different multiphase models to predict their behaviour in different types of MCHS. Kalteh et al. [19] applied the Eulerian-Eulerian two-phase equation to model the laminar forced convection in an isothermal two-parallel plate microchannel. Their results showed that the Eulerian two-phase model was in good agreement with experimental results based on the water-Cu nanofluid at Cu particle size between 30 and 100 nm and volume fraction up to 5%. Additionally, Kalteh et al. [20] experimentally and numerically investigated the thermal performance of water-γ-Al_2O_3 nanofluid in a wide rectangular microchannel heat sink using a two-phase Eulerian-Eulerian equation and the finite volume approach. Their numerical results, when compared with their experimental data, showed very good agreement with 7.42% maximum deviation. In another work, Mahdavi et al [21] applied both the Eulerian mixture model and the Lagrangian Discrete Phase Model (DPM) to study the heat transfer and the hydrodynamic characteristics of different nanofluids flow in a vertical tube. Other investigations in which homogeneous (single-phase), Eulerian-Eulerian (mixture, volume of fluid (VOF) and Eulerian) and Lagrangian models are used are presented here [22–24]. While the two-phase model has predicted with higher precision in some cases, several studies still implemented the single phase model in their numerical analyses of nanofluid in MCHS due to its much better convergence capability and lower computation power/accuracy ratio (i.e. higher computational efficiency). Besides, it has been established that with proper modelling (or experimental data) of thermal conductivity and viscosity, the single phase model could also be appropriately used for nanofluids thermo-flows problems [25].

The first generation microchannel heat sinks were based on the basic geometries such as rectangular channels [26], circular channels [27] and square channels [27–29]. The need for shape optimisation was because basic shapes such as rectangular and square channels were showing deficiencies as the energy density in compact spaces increased, therefore, trapezoidal channel [30], hexagonal channel [31] and other types of shapes were introduced. Subsequently, many researchers have introduced extended surfaces such as pin-fins and strip-fins. One of such works is the work of Ochende et al. [32] where they numerically investigated the effect of pin-fins inserts in a single and two-layered rectangular microchannel with different flow configurations. Their results showed that under increased heat load of 100–1000 W, the microchannel with pin-fins inserts performed better than the microchannel without pin-fins. Similarly, Adewumi et al. [33] numerically studied the thermal performance of a single layer microchannel with varying of the axial length and different micro pin-fin shapes. Their results showed that circular micro pin-fins were the most

efficient in maximizing the heat transfer from the MCHS base. Hong and Cheng [34] investigated the geometric optimisation of a laminar forced convection flow of pure water in an offset strip-fin microchannel heat sink. Their results showed that an optimized strip-fin size can minimized pressure drop, even when the global constraint of a maximum wall temperature is imposed.

Furthermore, a systematic review shows that the majority of the numerical investigations are geared towards the use of Newtonian nanofluid in the MCHS systems. As much as the Newtonian fluids, the non-Newtonian fluids have vital roles in many areas of industrial and engineering applications such as in the production of foods, drug production, drug delivery and crude oil drilling/processing. Besides, they are also used as heat transfer enhancer for compact heat exchangers in electronic modules. Therefore, the investigation of the application of non-Newtonian nanofluids in electronic module heat exchangers has economic and technological significance. Shahsavar et al. [35] investigated the heat transfer and optimized the entropy generation of non-Newtonian hybrid nanofluids in a concentric annulus. Hojjat et al. [36–38] employed water-based nanofluids of Al_2O_3, TiO_2, and CuO in the presence of 0.5 wt% CMC. They investigated the forced convection heat transfer of these non-Newtonian nanofluids in a tube under laminar and turbulent flow regimes. Their experimental result revealed an enhanced heat transfer coefficients for their nanofluids when compared with the base fluid. Baheri Islami et al. [39] experimentally investigated the thermal performance of a water-CMC based CuO nanofluid between two parallel plates with and without baffles for micromixing. Their results showed that the presence of nanoparticles, increasing Reynolds number and micromixer (baffle) increased the heat transfer (local and average) and the friction coefficient of the non-Newtonian nanofluid. Overall, the main mechanism for enhancing the heat transfer within the MCHS was the recirculation zones created by the micromixers fins.

To the best authors' knowledge, there is no investigation that addressed the performance of a non-Newtonian nanofluid in an offset strip-fins microchannel heat sink. This work investigates the hydrothermal performance and entropy generation characteristics of the water-CMC/CuO non-Newtonian nanofluid in an offset strip-fins microchannel heat sink. The goal is to optimize the strip fin geometry and study the influence of Reynolds number variation and volume fraction of CuO nanoparticle on the performance of the offset strip-fins MCHS from the viewpoint of both the first and the second thermodynamic law.

2. Geometric and mathematical model

2.1. Microchannel configuration and strip-fin parameters

The strip-fin employed in this study is of the offset type as depicted in Fig. 1. The geometric parameters of this microchannel heat sink (MCHS) are the length (L), the width (W) and the thickness (H), which are often fixed for a specific application. The geometric parameters of the strip-fins are given as fin length (L_s), fin interval (L_i), fin width (W_w), channel thickness (W_c) and channel height (H_c). Table 1 shows the corresponding dimensions of all the geometric parameters used in this study for the strip-fins microchannel. Indeed all the geometric parameters could be investigated, however, optimisation in this study will only be on the fin length (L_s) and fin interval (L_i), since one of the goals is to investigate the effect of fin on the performance of the MCHS. In addition, selecting the fin parameters for optimization will save computational efforts. Therefore, the following length ratios are defined:

$$\delta = \frac{L_i}{L_s} \tag{1}$$

$$\chi = \frac{\mathrm{L}}{L_i + L_s} \tag{2}$$

where δ is the ratio of fin offset to fin length and χ is the number of fins along the channel length. It should be noted that the fin width (W_w), channel thickness (W_c) and channel height (H_c) are assumed to be constant.

2.2. Governing equations

In this study, nanofluid prepared from the homogeneous mixture of CuO and water in the presence of 0.5 wt% CMC is employed as the working fluid in the strip-fins MCHS. The thermal performance and the entropy generation of this nanofluid are evaluated by assuming that the CuO nanoparticles are in thermal and dynamic equilibrium with the base fluid medium (water-CMC). It should be noted that the considered nanofluid is a non-Newtonian pseudo-plastic fluid [40]. The water-CMC/CuO nanofluid is an incompressible fluid, hence, the governing equations for the present study are:

Continuity equation:

$$\nabla.\left(\rho_{nf}\vec{\mathrm{u}}\right) = 0 \tag{3}$$

Momentum equation:

$$\nabla.\left(\rho_{nf}\vec{\mathrm{u}}\vec{\mathrm{u}}\right) = -\nabla \mathrm{p} + \nabla.\left(\mu_{nf}\nabla\vec{\mathrm{u}}\right) \tag{4}$$

Energy equation for the fluid region:

$$\nabla.\left(\rho_{nf}\vec{\mathrm{u}}\mathrm{c}_{\mathrm{p},nf}\mathrm{T}\right) = \nabla.\left(\mathrm{k}_{nf}\nabla\mathrm{T}\right) \tag{5}$$

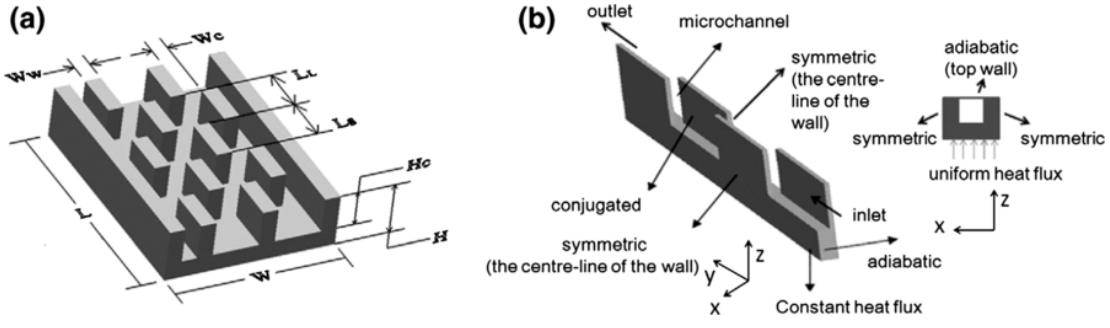

Fig. 1. Diagram of offset strip-fin MCHS with a description of its geometric parameters and imposed boundary conditions [34].

Table 1
Dimensions of geometric parameters for the offset strip-fin MCHS.

Geometric parameters	Dimensions (mm)
W	12
L	12
H	0.5
W_w	0.043
0.057	0.3
L_i	To be optimised
L_s	To be optimised

Energy equation for the solid:

$$\nabla.\left(k_s \nabla T_s\right) = 0 \tag{6}$$

where ρ is the density, $\vec{u}$ is the velocity, c_p is the specific heat capacity, T is the temperature, p is the pressure, k is the thermal conductivity, μ is the viscosity, and the subscripts *nf* and *s* denote to nanofluid and solid, respectively.

2.3. Boundary and initial conditions

At the bottom wall of the MCHS, a uniform heat flux ($q'' = 100\ \mathrm{W/cm^2}$) is imposed. All the remaining external walls are assumed to be perfectly thermally insulated with no any convective and radiation heat transfer with the surrounding medium (see Fig. 1b). At the inlet, the temperature of the nanofluid is assumed to be 300 K. The velocity at the inlet is taken to be uniformly distributed and other flow boundary conditions include no-slip at the internal walls and atmospheric pressure at the flow outlet.

Mathematically all the boundary conditions are represented as follows:

Flow inlet:

$$\vec{u} = \vec{u}_0; T = T_0 \tag{7a}$$

Flow outlet:

$$p = p_0 \tag{7b}$$

At the solid-fluid internal interface:

$$\vec{u} = 0; -k_{nf}\frac{\partial T}{\partial n} = q'' \tag{7c}$$

3. The nanofluid and its properties

The CuO nanoparticles are considered to be homogeneously dispersed within the water-CMC base fluid. The nanofluid effective density and specific heat capacity are calculated employing the following mixture models [40]:

$$\rho_{nf} = (1-\varphi)\,\rho_{bf} + \varphi\rho_p \tag{8}$$

$$c_{p,nf} = \frac{(1-\varphi)\,\rho_{bf} c_{p,bf} + \varphi\rho_p c_{p,p}}{\rho_{nf}} \tag{9}$$

where subscript *bf* and *p* refer to base fluid and nanoparticle, respectively.

The water-CMC/CuO nanofluid behaves as a pseudo-plastic fluid, hence the power law model is used to formulate its effective viscosity [40]:

$$\mu_{nf} = m\dot{\gamma}^{n-1} \tag{10}$$

where m is the consistency index, $\dot{\gamma}$ is the shear rate, and n is the power law index. Consistency index and power law index for water-CMC/CuO nanofluid at various concentrations are presented in Table 2. Additionally, the thermal conductivity of the water-CMC/CuO nanofluid at different nanoparticle concentrations is presented in Table 3.

4. Entropy generation

Generally, the local entropy generation also known as the total entropy is made up of two entropy generation components. First, is the entropy generated due to the friction and the second is the entropy generated due to the heat transfer in the system. Mathematically;

$$\dot{S}_T''' = \dot{S}_F''' + \dot{S}_H''' \tag{11}$$

$$\dot{S}_F''' = \frac{\mu_{nf}}{T}\left\{2\left[\left(\frac{\partial u_x}{\partial x}\right)^2 + \left(\frac{\partial u_y}{\partial y}\right)^2 + \left(\frac{\partial u_z}{\partial z}\right)^2\right] + \left(\frac{\partial u_x}{\partial y} + \frac{\partial u_y}{\partial x}\right)^2 + \left(\frac{\partial u_x}{\partial z} + \frac{\partial u_z}{\partial x}\right)^2 + \left(\frac{\partial u_z}{\partial y} + \frac{\partial u_y}{\partial z}\right)^2\right\} \tag{12}$$

$$\dot{S}_H''' = \frac{k_{nf}}{T}\left[\left(\frac{\partial T}{\partial x}\right)^2 + \left(\frac{\partial T}{\partial y}\right)^2 + \left(\frac{\partial T}{\partial z}\right)^2\right] \tag{13}$$

where $\dot{S}_T'''$ is the local total entropy generation rate in the MCHS, $\dot{S}_F'''$ is the local frictional entropy generation rate and $\dot{S}_H'''$ is the local thermal entropy generation rate. The global entropy generation within the system is the integration of the total entropy over the whole domain. Similarly, the global entropy generation by heat transfer and friction can

Table 2
Consistency and power law indexes of the water-CMC/CuO nanofluid [36].

φ (%)	m	n
0	0.145	0.542
0.5	0.144	0.541
1.0	0.142	0.537
1.5	0.130	0.546
3.0	0.114	0.571

Table 3
Thermal conductivity of the water-CMC/CuO nanofluid [37].

φ (%)	Thermal conductivity, k_{nf} (W/m K)
0	0.613
0.5	0.602
1.0	0.616
1.5	0.622
3.0	0.764

be calculated as presented in Eq. (14);

$$\dot{S}_T = \int \dot{S}_T''' dV; \dot{S}_H = \int \dot{S}_H''' dV; \dot{S}_F = \int \dot{S}_F''' dV \tag{14}$$

5. Data reduction

The overall objective of a heat sink is to remove as much as possible the effect of the imposed heat flux by keeping the temperature of the base of the heat sink as low as possible. It is a general requirement for the flat surface of the MCHS (the point of input of heat flux) to produce a uniform surface temperature distribution and remove any hot spot situation for the effective performance of the electronic component. To quantitatively determine the cooling performance of the MCHS, the difference between the maximum and minimum temperature of the base of the MCHS and the pressure drop across the microchannel will be evaluated. Therefore, the following evaluation criteria are defined:

$$\theta = \frac{T_s^{\max} - T_s^{\min}}{q''} \tag{15}$$

Eq. (15) is the temperature non-uniformity per unit flux, used to indicate the temperature uniformity/non-uniformity on the CPU surface. A higher value of θ means a less uniform temperature distribution. The thermal resistance of the nanofluid is also vital in monitoring the performance of the MCHS [41]. Therefore, the goal is to achieve as much as possible a low thermal resistance which is dependent on the mean surface temperature of the MCHS. From Eq. (16) it could be inferred that a low mean surface temperature indicates there is an efficient heat transfer within the MCHS. Consequently, one of the yardsticks for measuring the best performance will be a low value of θ and R.

$$R = \frac{T_s^{mean} - T_{nf}^{in}}{q''} \tag{16}$$

The pumping power of the working fluid is related to the cost of operation of the MCHS among other issues. Hence, the performance criteria should include monitoring of the pumping power requirement of the heat sink vis a vis the nanofluid that is employed. The pumping power required is obtained using Eq. (17).

$$P_{pump} = \dot{Q}\Delta p \tag{17}$$

where $\dot{Q}$ is the volumetric flow rate of the nanofluid in the MCHS. It is general knowledge that the addition of nanoparticles increases both the viscosity and thermal conductivity of the nanofluid. This may increase both the thermal performance and the pumping cost, as such the ratio of the relative heat transfer coefficient to the relative pressure drop across the MCHS is also defined as the performance evaluation criterion (PEC) as shown:

$$PEC = \frac{h_{nf}/h_{bf}}{\Delta p_{nf}/\Delta p_{bf}} \tag{18}$$

Eq. (19) is used to determine the heat transfer coefficient for the MCHS adopting the methodology implemented by Bahiraei and Heshmatian [41].

$$h = \frac{q''}{T_s^{mean} - T_{nf}^{mean}} \tag{19}$$

The Reynolds number for non-Newtonian power law fluids is defined as:

$$Re = \frac{\rho_{nf} D_h^n u_{in}^{2-n}}{m} \tag{20}$$

where D_h is the hydraulic diameter obtained as $D_h = 2H_cW_c/(H_c + W_c)$ and u_{in} is the nanofluid inlet velocity.

6. Numerical technique and validation

The present study considers the laminar convective heat transfer of water-CMC/CuO nanofluid in an offset strip-fins microchannel. The flow physics was set up in a commercial CFD software ANSYS FLUENT®. The governing equations with the associated boundary conditions were solved using the finite volume method. The momentum and the energy equations were solved employing the second order upwind scheme. The pressure and the velocity fields were coupled using the SIMPLE algorithm. The accuracy of the solution to convergence was monitored at 10^{-6} for the continuity, x-velocity, y-velocity, z-velocity and the energy equation.

6.1. Mesh study

The geometry of this study was discretised using a structured mesh based on a rectangular grid and it was generated throughout the computational domain as shown in Fig. 2. In order to substantiate the independence between the grid and the numerical results and choosing an appropriate mesh configuration, six different combinations of node numbers (six cases) have been examined by comparing the pressure drop and average convective heat transfer coefficient for the nanofluid at $\varphi = 3\%$, $Re = 700$, $\delta = 1$ and $\chi = 16$. As shown in Table 4, there is no significant difference between the results of case 5 and case 6. The error in the pressure drop and heat transfer coefficient results is 1.29% and 1.11%, respectively. Therefore, case 5 (32, 145 and 2400 nodes in x, y and z directions, respectively) is used for the rest of numerical computations.

6.2. Validation

In order to validate and ensure the accuracy of the numerical simulation, the difference between the maximum and the minimum values of the CPU surface temperature ($\Delta T_s = T_s^{\max} - T_s^{mean}$), obtained in the present work was compared to the work of Hong and Cheng [34] for the flow of deionized water inside the offset strip-fins MCHS with different χ values and $\delta = 1$. The coolant mass flow rate was varied to guarantee the same $T_s^{\max}$ as that of Hong and Cheng [34]. This comparison is illustrated in Table 5, and it can be observed that there is an appropriate consistency between the results of the present work and the one existing in the literature. Moreover, the convective heat transfer coefficient obtained in the current study was compared to the experimental findings of Khoshvaght-Aliabadi et al. [42] for flow of water-Cu nanofluid flow in an offset strip-fins channel. Table 6 shows that the comparison is excellent.

7. Results and discussion

This study conducted a numerical simulation to investigate the hydrothermal and entropy generation characteristics of a non-Newtonian

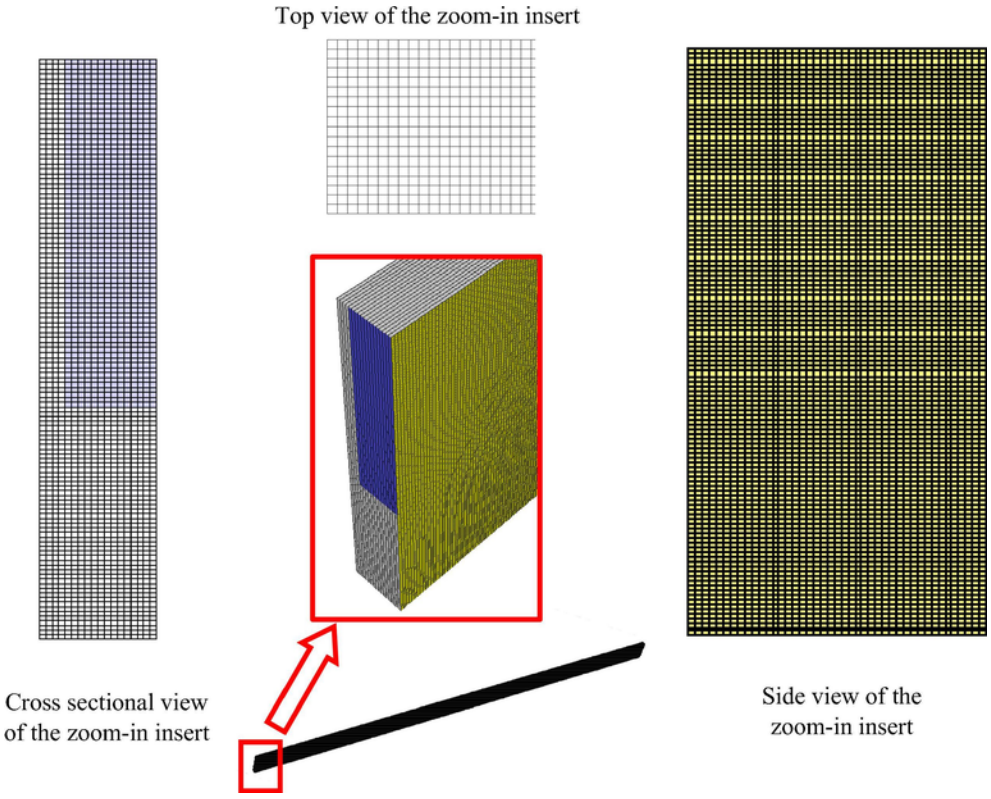

Fig. 2. The structured mesh of the computational domain and the zoom-in insert of the domain along with the three side views.

Table 4
Mesh independence study monitored with the pressure drop and average convective heat transfer coefficient for flow of nanofluid at $\varphi = 3\%$, $Re = 700$, $q'' = 100\ W/cm^2$, $\delta = 1$ and $\chi = 16$.

	CASE 1	CASE 2	CASE 3	CASE 4	CASE 5	CASE 6
Grid size	20 × 125 × 2400	22 × 135 × 2400	32 × 145 × 2200	32 × 145 × 2300	32 × 145 × 2400	32 × 145 × 2500
Δp (kPa)	353.87	375.54	397.45	412.12	426.83	432.34
h $(W/m^2\ K)$	197,123	207,127	212,555	216,678	217,493	219,898

Table 5
Results obtained from the present work compared with those of Hong and Cheng [34].

χ	ΔT_s [34]	ΔT_s (present)	Error (%)
2	18.5	18.9	2.16
4	17.7	18.3	3.39
8	18.5	18.8	1.62
20	20.7	21.1	1.93

Table 6
Results obtained from the present work compared with those of Khoshvaght-Aliabadi et al. [42] at $\varphi = 0.4\%$.

Q̇(litres/min)	h (W/m^2 K) [42]	h (W/m^2 K) (present)	Error (%)
2	256	270.12	5.52
3	293	312.56	6.68
4	332	354.23	6.71
5	365	386.01	5.76

nanofluid with CuO nanoparticles runs through an offset strip-fin MCHS. The proposed microchannel was situated on a CPU to cool it down. The simulations were performed for various concentrations (0, 0.5, 1 and 3%), Reynolds numbers (100, 300, 500 and 700), ratios of fin offset to fin length (0.5, 1 and 2), and fin numbers along the channel length (4, 6, 8 and 16). Initially, the effects of concentration and Reynolds numbers on the performance of MCHS from the first law perspective are investigated and later, the effects of these parameters on the MCHS performance are discussed from the second law viewpoint.

Fig. 3 displays contours of velocity, strain rate and viscosity at the mid-plane cross-section through MCHS ($y = 0.15$ mm) for $\varphi = 3\%$, $Re = 700$, $\delta = 1$ and $\chi = 16$. For clear observation, due to the slender ratio of the proposed geometry, the prepared contours are displayed at the distance of 2.81–3.56 mm from the inlet (2.81 mm $< z <$ 3.56 mm). As seen, the flow accelerates by passing through the narrow passage (between two fin corners) and decelerates by increasing the width of the passage. This flow pattern leads to high-velocity gradients at the edges of fins (narrow passage regions) and consequently viscosity decrease in those regions while by passing the narrow passages, the fluid viscosity increases due to dropping in velocity gradients.

Fig. 4 illustrates the trend of convective heat transfer coefficient in heat sink in terms of nanofluid concentration at different Reynolds numbers for $\delta = 1$ and $\chi = 16$. As shown, convective heat transfer coefficient increases with the increase of Reynolds number which is more pronounced at low Reynolds numbers. For example, by increasing Reynolds number from 100 to 700 at concentrations of 0 and 3%, the percentage of the convective heat transfer coefficient increase are 49.93 and 55.7, respectively. The convective heat transfer coefficient is proportional to the ratio of the thermal conductivity to the thermal

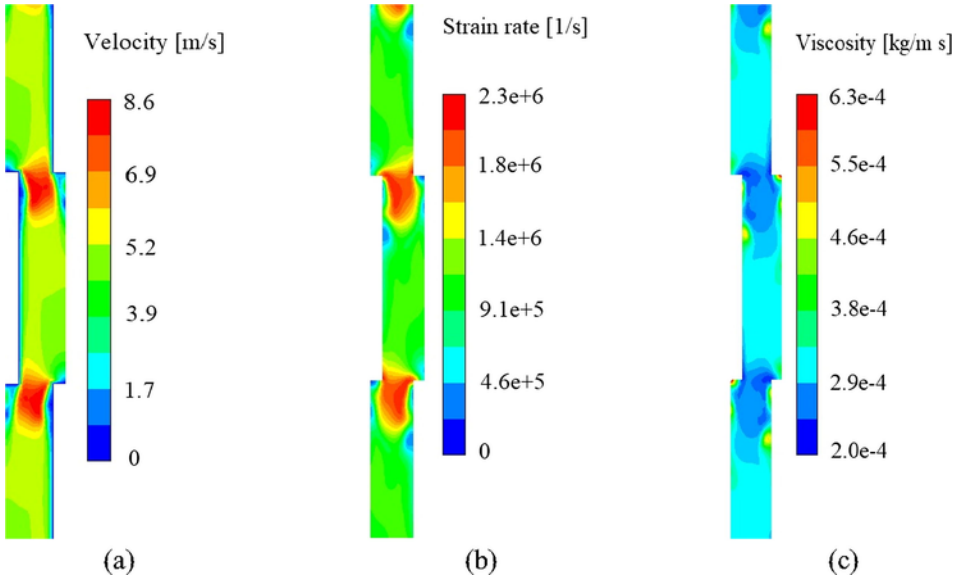

Fig. 3. Contours of (a) velocity, (b) strain rate, and (c) viscosity at the mid-plane cross section of the heat sink ($y = 0.15$ mm, $2.81\,\text{mm} < z < 3.56\,\text{mm}$) for $\varphi = 3\%$, $Re = 700$, $\delta = 1$ and $\chi = 16$.

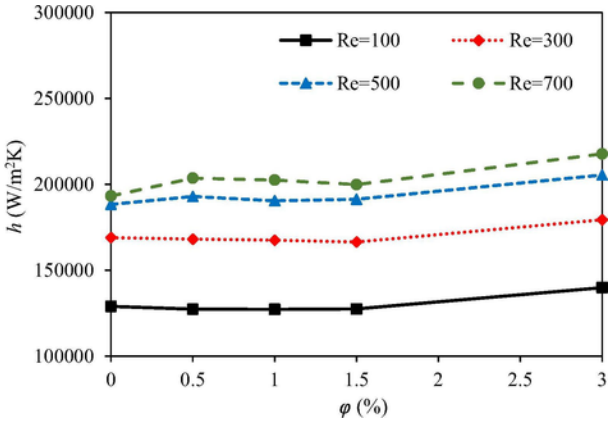

Fig. 4. The effect of Reynolds number on convective heat transfer coefficient vs. nanoparticle concentration at $\delta = 1$ and $\chi = 16$.

boundary layer thickness ($\text{h k}/\delta_t$). The increase of Reynolds number at a constant nanoparticle concentration leads to a decrease in hydraulic boundary layer thickness and consequently decrease in thermal boundary layer thickness which cause an increase in the convective heat transfer coefficient.

Fig. 4 also displays the impact of nanoparticle concentration on convective heat transfer coefficient which as seen is less than the Reynolds number impact (curves are almost flat). This effect is more pronounced at low Reynolds numbers (100 and 300) with concentration up to 1.5%. Indeed, for analysing the effect of nanoparticle concentration on convective heat transfer coefficient, one has to consider the effect of following parameters simultaneously: thermal boundary layer thickness, thermal conductivity and non-Newtonian nature of the fluid. The obtained results demonstrate that at a constant Reynolds number, increasing nanoparticle concentration to 1.5% and beyond 1.5% to 3% respectively leads to a decrease and increase in both the nanofluid velocity and the convective heat transfer coefficient (please consult with the earlier discussion on the influence of velocity on convective heat transfer coefficient). In addition, as shown in Table 3, increasing nanoparticle concentration up to 0.5% and from 0.5% to 3% respectively leads to decrease and increase of thermal conductivity which has a direct effect on convective heat transfer coefficient. It is noteworthy that due to shear thinning nature of the nanofluid, by decreasing the hydraulic boundary layer thickness (increasing velocity gradient), the viscosity decreases which leads to flow acceleration close to the solid walls and consequently enhancing heat transfer rate. Therefore, in a word, surveying the effects of nanoparticle concentration in the proposed nanofluid is not straight forward and demands considering all different parameters together including thermal boundary layer thickness, thermal conductivity and non-Newtonian nature of the fluid.

Fig. 5 shows the effects of nanoparticle concentration on the average temperature of the CPU surface for $\delta = 1$ and $\chi = 16$. As seen, the CPU surface temperature favourably drops with increasing Reynolds number. For example, by increasing Reynolds number from 100 to 700 at concentrations of 0 and 3%, the percentage of the CPU surface average temperature respectively drops by 1.76 and 1.79%. These trends can be attributed to the fact that convective flow enhances with an increase in the Reynolds number. Furthermore, as Fig. 5 displays the non-Newtonian nanofluid with nanoparticle concentration of 3% has the best cooling performance.

The effects of nanoparticle concentration and Reynolds number on the temperature distribution of the nanofluid at the mid-plane cross-section of the MCHS ($y = 0.15$ mm, $2.81\,\text{mm} < z < 3.56\,\text{mm}$) for $\delta = 1$

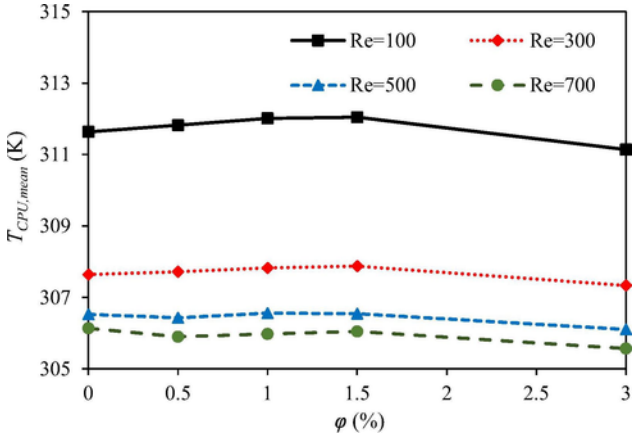

Fig. 5. The effect of Reynolds number on the average temperature of the CPU surface vs. nanoparticle concentration at $\delta = 1$ and $\chi = 16$.

and $\chi = 16$ are illustrated in Fig. 6. As expected, the temperature of nanofluid along the length of the channel gradually raises (due to heat transfer with heat sink walls). The results show that increasing nanoparticle concentration up to 1% will increase the maximum nanofluid temperature while by dissolving more nanoparticles (nanoparticle concentration up to 3%), the maximum nanofluid temperature drops. In addition, as displayed, the maximum nanofluid temperature decreases with the increase of Reynolds number which can be attributed to enhancing convective flow with increasing Reynolds number.

One of the crucial points in designing of electronic equipment is avoiding hotspot which has a significant effect on the lifetime and performances of the equipment. Therefore, in the performance investigation of electronic equipment, the designers should pay attention to the temperature of the electronic stuff not to exceed a specific limit. Fig. 7 displays the influence of nanoparticle concentrations on the maximum temperature of the CPU surface at different Reynolds numbers for $\delta = 1$ and $\chi = 16$. As seen, with increasing Reynolds number, the maximum temperature of the CPU surface significantly drops while nanofluid concentration, except at 3%, which does not have a significant influence on the maximum temperature of the CPU surface.

Addition of nanoparticles to a base fluid would have a favourable effect which is enhancing the heat transfer rate, however, it has a negative effect as well. Indeed, nanoparticle addition to a base fluid will increase the pure fluid viscosity and consequently leads to more pressure drop and pumping power cost of the system. Fig. 8 illustrate the effects of nanoparticle concentrations at different Reynolds number for $\delta = 1$ and $\chi = 16$. As shown, increase in the Reynolds number results in a remarkable increase in the pumping power. Besides, as displayed, pumping power will be reduced up to 1% nanoparticle concentration and then will increase by adding more particles to the nanofluid (beyond 1%). To analyse this behaviour, the following facts have to be considered. According to Darcy's equation ($\Delta p = f\frac{L}{D_h}\frac{\rho u_{in}^2}{2}$, where f is the fric-

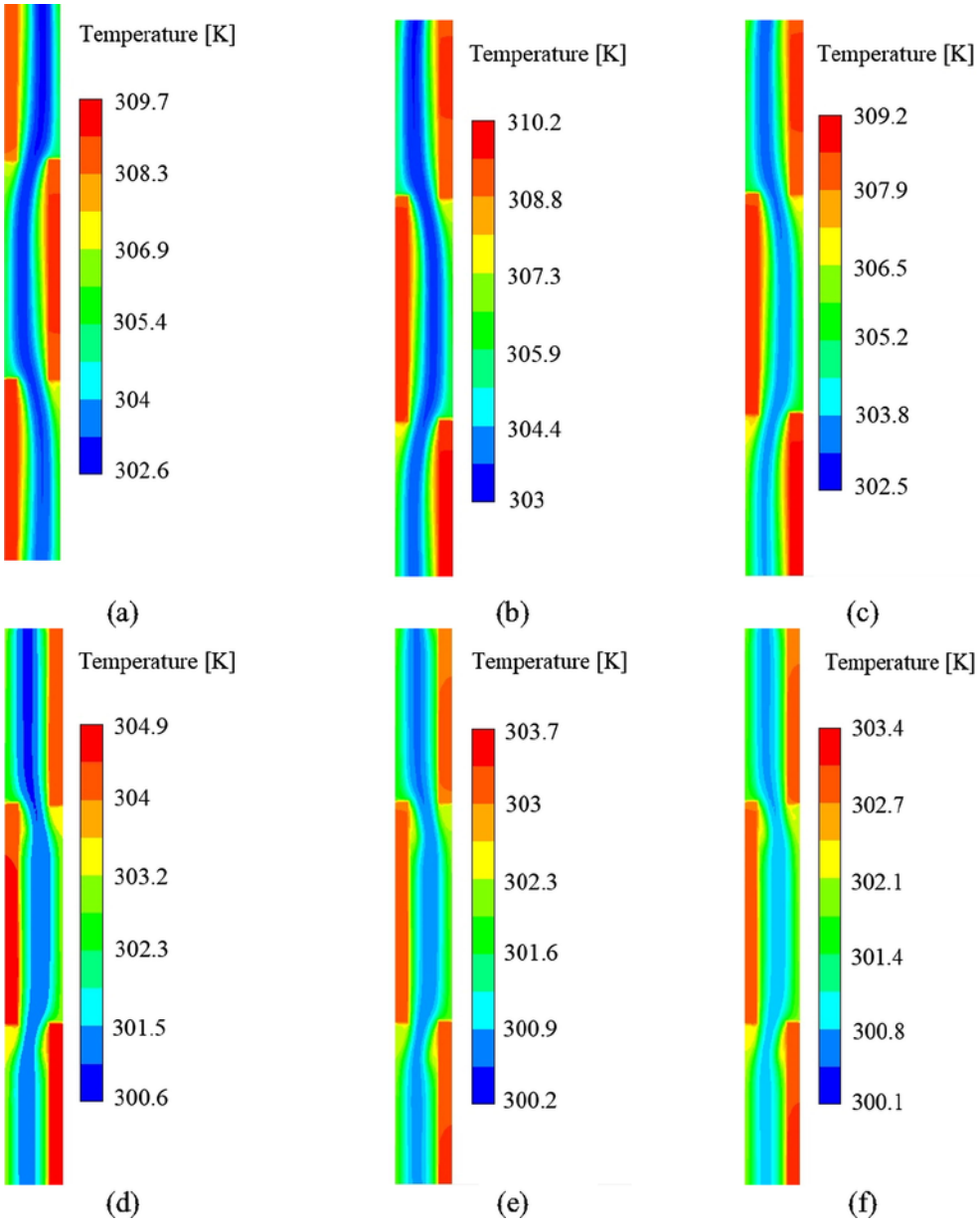

Fig. 6. Contours of temperature of the nanofluid at the mid-plane cross section of the heat sink ($y = 0.15$ mm, 2.81 mm $< z <$ 3.56 mm) for $\delta = 1$, $\chi = 16$ and (a) $\varphi = 0\%$&$Re = 100$, (b) $\varphi = 1\%$&$Re = 100$, (c) $\varphi = 3\%$&$Re = 100$, (d) $\varphi = 3\%$&$Re = 300$, (e) $\varphi = 3\%$&$Re = 500$ and (f) $\varphi = 3\%$&$Re = 700$.

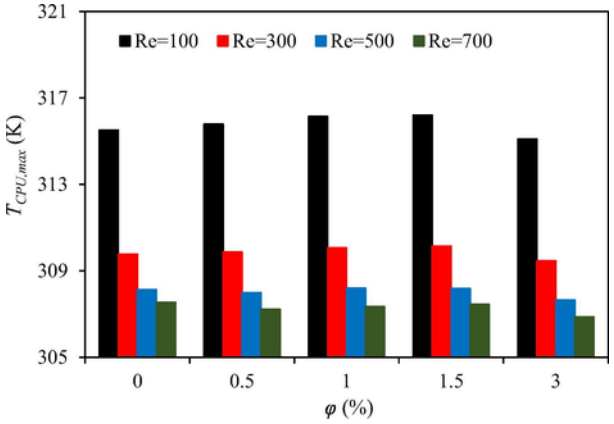

Fig. 7. Maximum temperature of CPU surface in terms of nanoparticle concentration and Reynolds number for $\delta = 1$ and $\chi = 16$.

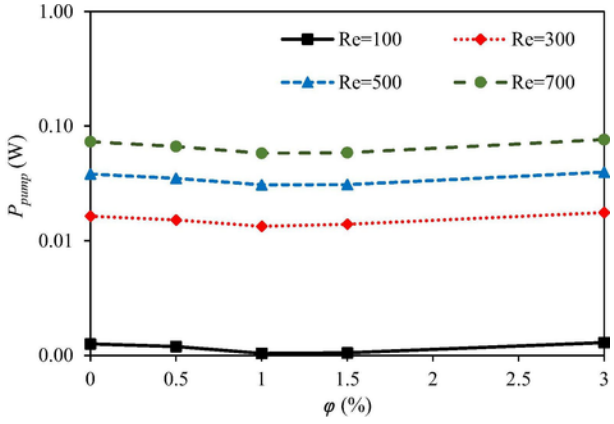

Fig. 8. Pumping power in terms of nanoparticle concentration and Reynolds number for $\delta = 1$ and $\chi = 16$.

tion factor defined as $f = \frac{64}{Re}$ [43]) and due to constant parameters of the study (friction factor, hydraulic diameter and length of the microchannel) in a Reynolds number, pressure drop will be the function of the nanofluid velocity and density. As results shown, increase in the nanoparticle concentration leads to an increase in both the nanofluid density and viscosity. Up to 1.5% nanoparticle concentration, increase in the density is more dominant than the increase in the viscosity, and consequently, the nanofluid decelerates while beyond 1.5% concentration the counter fact governs and the fluid accelerates. Therefore, based on Fig. 8, one can conclude that for nanoparticle concentrations up to 1%, the effects of a reduction in velocity are dominant, leading to reduction in pressure drop, while for higher concentrations, the effects of enhancing in nanofluid density are dominant and pressure drop increases.

Thermal resistance (R) and uniformity of temperature distribution (θ) are two important parameters in the investigation of heat sink performance. Figs. 9 and 10 respectively display the effects of nanofluid concentration on thermal resistance and uniformity of temperature in CPU cooling for different Reynolds numbers at $\delta = 1$ and $\chi = 16$. The results show that both R and θ are favourably affected (reduction in values) by increasing in Reynolds number while the nanofluid concentration, except 3%, does not have significant effect on those parameters.

Fig. 11 displays the effects of nanoparticles concentration on PEC at different Reynolds numbers for $\delta = 1$ and $\chi = 16$. PEC is the most important criteria, which a designer has to consider in picking a suitable nanofluid for a heat sink. Represented results in Fig. 11 show that PEC

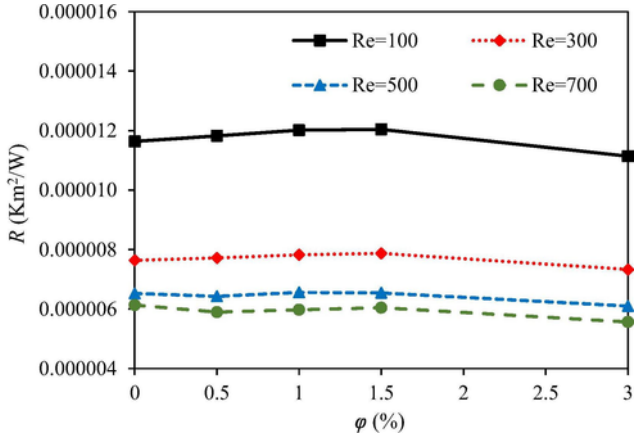

Fig. 9. Parameter R in terms of nanoparticle concentration and Reynolds number for $\delta = 1$ and $\chi = 16$.

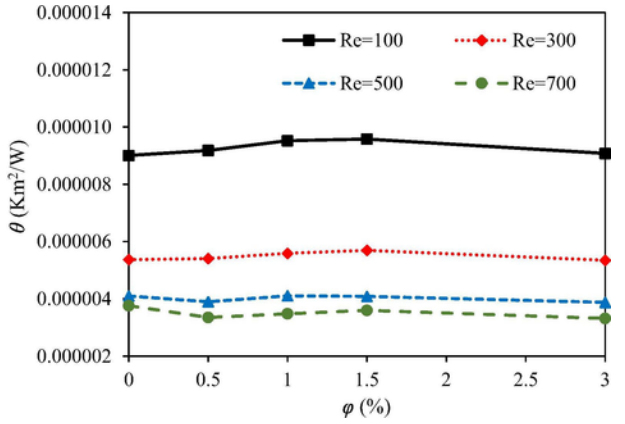

Fig. 10. Parameter θ in terms of nanoparticle concentration and Reynolds number for $\delta = 1$ and $\chi = 16$.

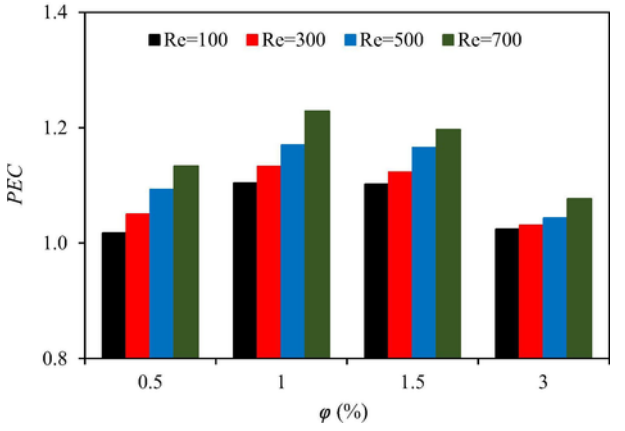

Fig. 11. PEC of nanofluid in terms of nanoparticle concentration and Reynolds number for $\delta = 1$ and $\chi = 16$.

boosts with an increase in the Reynolds number. As shown, for the non-Newtonian nanofluid, the maximum PEC (1.23) takes place at 1% nanoparticle concentration and Reynolds 700.

At the end of this section (discussion of results from the first law perspective), a survey is represented in Fig. 12 to see how PEC of the nanofluid varies with δ and χ at $\varphi = 1\%$ and $Re = 700$. As shown, the trend of the PEC is descending with increasing of χ. At a constantδ, with increasing inχ, the number of strip-fins along the flow direction increases which leads to augmentation in the flow disturbance and the

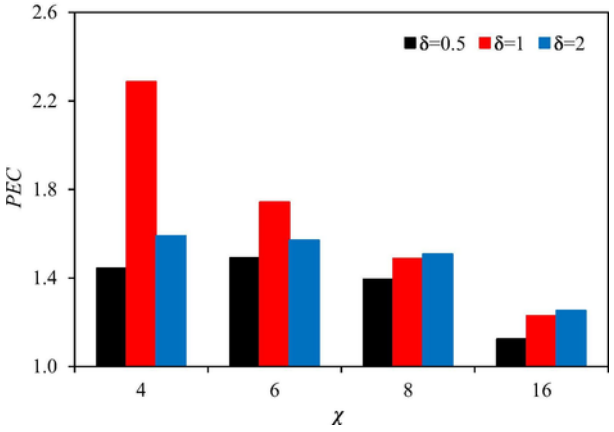

Fig. 12. PEC of nanofluid in terms of number of fins along the flow direction and the ratio of fin length to fin interval.

break-up of boundary layer, and consequently, pressure drop and heat transfer increase. As seen in Fig. 12, the ratio of increase in heat transfer to pressure drop for nanoparticle concentration of 1% at Reynolds number of 700 is more than the base fluid. In addition, as displayed, the PEC is always more than 1. Furthermore, Fig. 12 reveals that the maximum achievable PEC for the proposed non-Newtonian nanofluid takes place in the case of $\delta = 1$ and $\chi = 6$ which equals to 2.29.

Fig. 13 displays the thermal, frictional and total entropy generation rates in the mid-plane section of the MCHS ($y = 0.15$ mm, 2.81 mm $< z <$ 3.56 mm) for $\varphi = 3\%$, $Re = 700$, $\delta = 1$ and $\chi = 16$. As shown, the maximum rate of entropy generation occurs at the corner of fins which is due to the higher velocity and temperature gradients at those regions.

Fig. 14 illustrates the effects of nanoparticle concentration and Reynolds number on the global frictional entropy generation rate at $\delta = 1$ and $\chi = 16$. As displayed, increase in the Reynolds number leads to significant augmentation of global frictional entropy generation rate which can be attributed to reduction in average fluid temperature as well as hydraulic boundary layer thickness and consequently increase in the velocity gradient. In addition, Fig. 14 shows that an increase in the nanoparticle concentration up to 1.5% does not have a significant effect on the global frictional entropy generation rate, in particular at Reynolds numbers of 100 and 300. However, beyond 1.5%, the global frictional entropy generation rate increases with increasing nanoparticle concentration at all Reynolds numbers. This behaviour can be attributed to the following facts. Firstly, increasing nanoparticle concentration up to 1.5% leads to a decrease in the average temperature of nanofluid, and therefore, an increase in the global frictional entropy generation rate while reverse trends take place for higher concentrations. Secondly, augmentation in nanoparticle concentration up to 1% causes a decrease in the nanofluid viscosity, and consequently, a decrease in the global frictional entropy generation rate while the opposite is true for nanoparticle concentrations higher than 1%. Last but not the least, according to Table 2, the non-Newtonian characteristic of the nanofluid is boosted with increasing in nanoparticle concentration up to 1% while it is weakened by a further increase in the nanoparticle concentration. Hence, nanoparticle concentration up to 1.5% leads to a flatter velocity profile (velocity gradient reduction) and decrease in the global frictional entropy generation rate while reverse trends take place for higher concentrations.

The effects of nanoparticle concentration and Reynolds number on the global thermal entropy generation rate at $\delta = 1$ and $\chi = 16$ are displayed in Fig. 15. It is observed that the global thermal entropy generation rate reduces with increasing Reynolds number. For example, by increasing in Reynolds number from 100 to 700, the global thermal entropy generation rate of base fluid and nanofluid with nanoparticle concentration of 3% increases by 62.1 and 62.4%, respectively. This is due to the formation of stronger vortices around the fins at higher Reynolds numbers, which leads to an increase in the temperature gradients and thus a rise in the global thermal entropy generation rate. Besides, as shown, the global thermal entropy generation rate does not significantly change with nanoparticle concentration up to 1.5%, while, after that the global thermal entropy generation rate decreases at all Reynolds numbers. As seen, at nanoparticle concentration of 3%,

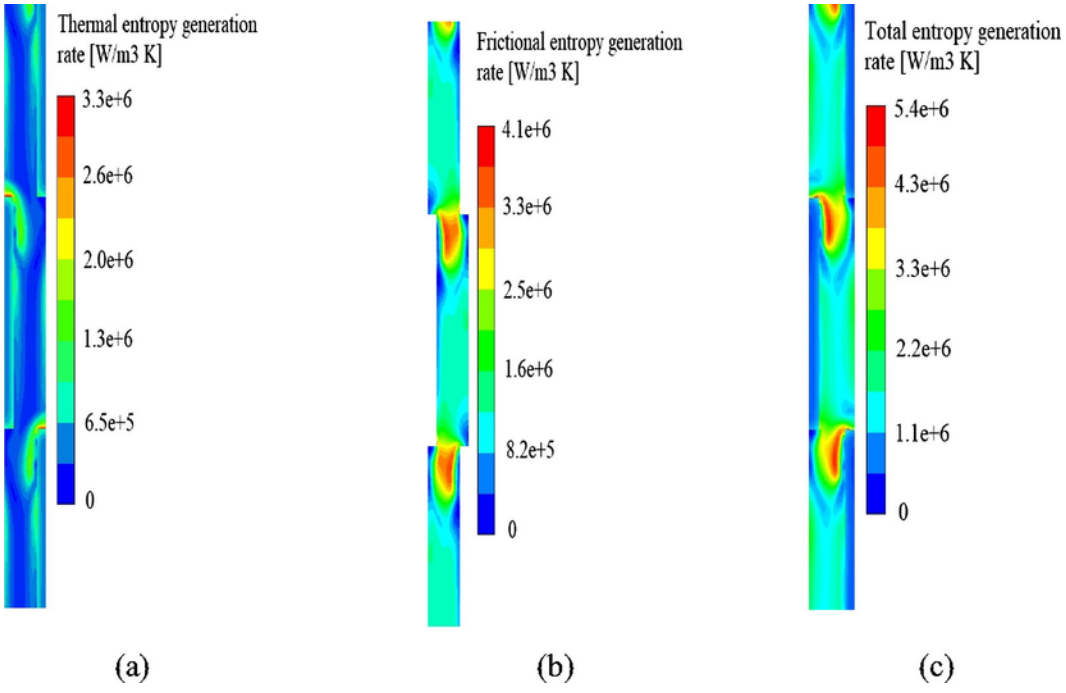

Fig. 13. Contours of (a) thermal, (b) frictional, and (c) total entropy generation rates at the mid-plane cross section of the heat sink ($y = 0.15$ mm, 2.81 mm $< z <$ 3.56 mm) for $\varphi = 3\%$, $Re = 700$, $\delta = 1$ and $\chi = 16$.

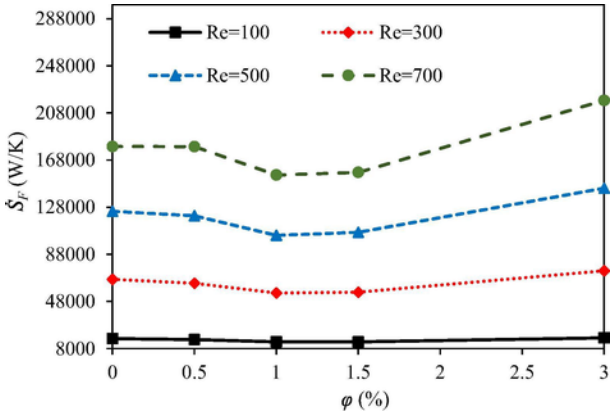

Fig. 14. Frictional entropy generation rate of nanofluid as a function of nanoparticle concentration with the effect of Reynolds number for $\delta = 1$ and $\chi = 16$.

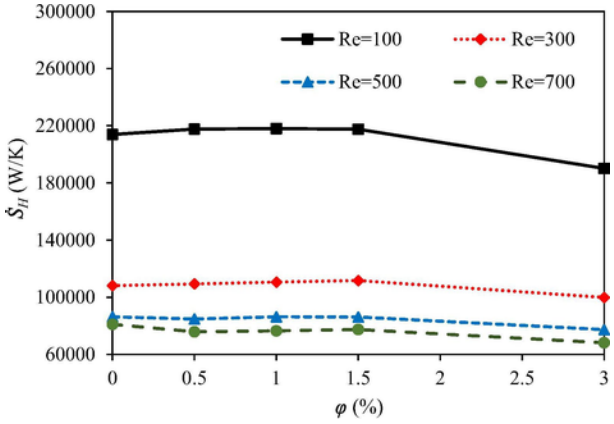

Fig. 15. Thermal entropy generation rate of nanofluid in terms of nanoparticle concentration and Reynolds number for $\delta = 1$ and $\chi = 16$.

the nanofluid has a lower global thermal entropy generation rate than the base fluid. To analyse this behaviour, all three parameters of the thermal conductivity, fluid average temperature and temperature gradient have to be investigated. As listed in Table 3, increasing nanoparticle concentration up to and beyond 0.5% respectively leads to decrease and increase in the thermal conductivity of nanofluid, and consequently, decrease and increase in the global thermal entropy generation rate. In addition, at a constant Reynolds number, increase in the nanoparticle concentration leads to a reduction in Prandtl number and consequently, augmentation in the thermal boundary layer thickness. Hence, the temperature gradient reduces by increasing the nanoparticle concentration leading to an increase in the global thermal entropy generation rate. Last but not the least, as discussed, the nanofluid average temperature increases and decreases respectively up to and after 1.5% concentration. Hence, according to Fig. 15, the effects of three governing parameters (thermal conductivity, fluid average temperature and temperature gradient) on the global thermal entropy generation rate neutralize each other up to 1.5% nanoparticle concentration, but beyond this point, the effect of temperature gradient reduction is dominant and the global thermal entropy generation rate reduces.

The effects of nanoparticle concentration and Reynolds number on the global total entropy generation rate at $\delta = 1$ and $\chi = 16$ are displayed in Fig. 16. As shown, increase in the Reynolds number from 100 to 300, leads to a significant reduction in the global total entropy generation rate while more increase in the Reynolds number enhances the global total entropy generation rate. In addition, as shown in Fig. 16, for Reynolds numbers beyond 300, up to 1% nanoparticle concentration, the global total entropy generation rate drops while beyond this point the global total entropy generation rate increase. However, for Reynolds numbers lower than 300, the trend of variations of global total entropy generation rate with nanoparticle concentration is completely reverse. In a word, the minimum global total entropy generation rate of the considered nanofluid in the case of $\delta = 1$ and $\chi = 4$ takes place at nanoparticle concentration of 1% and Reynolds number of 300.

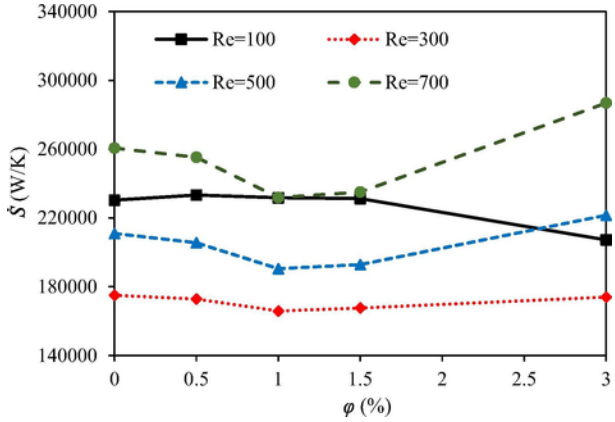

Fig. 16. Total entropy generation rate of nanofluid in terms of nanoparticle concentration and Reynolds number for $\delta = 1$ and $\chi = 16$.

At the end of this section (discussion of results from the second law perspective), an investigation on the effects of δ and χ on the global total entropy generation rate at $\varphi = 1\%$ and $Re = 300$ is depicted in Fig. 17. As shown, the trend of the total entropy generation rate versus δ and χ does not have a specific pattern. For example, in the case of $\delta = 0.5$, the global total entropy generation rate improves with increase of χ, while the opposite trend is observed in the case of $\delta = 2$. According to the results, the minimum global total entropy generation rate takes place in the case of $\delta = 1$ and $\chi = 6$ and equals to 161706.3 W/K, which is 2.7% less than that of the base fluid at the same conditions.

In conclusion, from the viewpoint of both the first and the second thermodynamic law, the best performance of the system take places at nanoparticle concentration of 1%, which has the lowest power law index (see Table 2) and consequently shows the most sever shear thinning behaviour. Therefore, one can conclude that the non-Newtonian nanofluid has great potential in cooling of electronic equipment which can be explored in future researches.

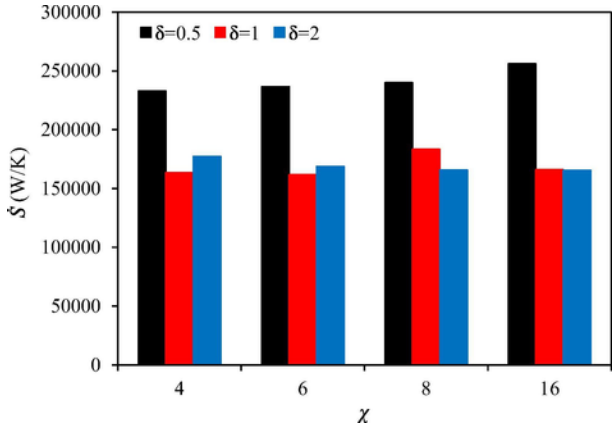

Fig. 17. Total entropy generation rate of nanofluid in terms of number of fins along the flow direction and the ratio of fin length to fin interval.

8. Conclusion

The present numerical study investigates the hydrothermal and entropy generation characteristics of the non-Newtonian water-CMC/CuO nanofluid in an offset strip-fin MCHS. The impacts of nanoparticles concentration and Reynolds number on the convective heat transfer coefficient, CPU surface temperature, nanofluid temperature, pumping power, as well as the thermal, frictional and total entropy generation rates are numerically assessed. The inferences from the investigations are as follows:

- The considered nanofluid displays better convective heat transfer coefficient compared to the base fluid, especially at high Reynolds numbers and nanoparticle concentrations.
- The cooling uniformity enhances by increasing nanoparticle concentration beyond 1% as well as increasing Reynolds number.
- The CPU surface temperature reduces by augmenting either nanoparticle concentration beyond 1.5% or Reynolds number.
- The pumping power decreases by increasing nanoparticle concentration up to 1% as well as increasing Reynolds number.
- With increase in Reynolds number and nanoparticle concentration to more than 1.5%, the thermal resistance reduces.
- From the first law perspective, the non-Newtonian water-CMC/CuO nanofluid shows the best performance in the considered offset strip-fins MCHS in the case of $\varphi = 1\%$, $Re = 700$, $\delta = 1$ and $\chi = 4$.
- The global frictional entropy generation rate increases by increasing Reynolds number. In addition, increasing nanoparticle concentration up to and beyond 1% respectively leads to a decrease and increase in the global frictional entropy generation rate.
- The global thermal entropy generation rate reduces with enhancing Reynolds number. Additionally, for nanoparticle concentrations higher than 1%, the global thermal entropy generation rate decreases with increase in concentration.
- The lowest global total entropy generation rate of the non-Newtonian water-CMC/CuO nanofluid in the examined offset strip-fins MCHS occurs in the case of $\varphi = 1\%$, $Re = 300$, $\delta = 1$ and $\chi = 6$.

Acknowledgements

The authors would like to thank Dr. Masoud Afrand (Najafabad Branch, Islamic Azad University, Najafabad, Iran) for his comments and discussion.

References

[1] Y. Gao, H. Wang, A.P. Sasmito, A.S. Mujumdar, Measurement and modeling of thermal conductivity of graphene nanoplatelet water and ethylene glycol base nanofluids, Int. J. Heat Mass Transf. 123 (2018) 97–109, https://doi.org/10.1016/j.ijheatmasstransfer.2018.02.089.

[2] A. Kakavandi, M. Akbari, Experimental investigation of thermal conductivity of nanofluids containing of hybrid nanoparticles suspended in binary base fluids and propose a new correlation, Int. J. Heat Mass Transf. 124 (2018) 742–751, https://doi.org/10.1016/j.ijheatmasstransfer.2018.03.103.

[3] M. Keyvani, M. Afrand, D. Toghraie, M. Reiszadeh, An experimental study on the thermal conductivity of cerium oxide/ethylene glycol nanofluid: developing a new correlation, J. Mol. Liq. 266 (2018) 211–217, https://doi.org/10.1016/j.molliq.2018.06.010.

[4] M.M. Hayat, A. Irannezhad, Experimental investigation on the competition between enhancement of electrical and thermal conductivities in water-based nanofluids, J. Mol. Liq. 268 (2018) 169–175, https://doi.org/10.1016/j.molliq.2018.07.022.

[5] A. Naddaf, S.Z. Heris, Experimental study on thermal conductivity and electrical conductivity of diesel oil-based nanofluids of graphene nanoplatelets and carbon nanotubes, Int. Commun. Heat Mass Transf. 95 (2018) 116–122, https://doi.org/10.1016/j.icheatmasstransfer.2018.05.004.

[6] H.D. Koca, S. Doganay, A. Turgut, I.H. Tavman, R. Saidur, I.M. Mahbubul, Effect of particle size on the viscosity of nanofluids: a review, Renew. Sust. Energ. Rev. 82 (2018) 1664–1674, https://doi.org/10.1016/j.rser.2017.07.016.

[7] W.M. Hasona, A.A. El-Shekhipy, M.G. Ibrahim, Combined effects of magnetohydrodynamic and temperature dependent viscosity on peristaltic flow of Jeffrey nanofluid through a porous medium: applications to oil refinement, Int. J. Heat Mass Transf. 126 (2018) 700–714, https://doi.org/10.1016/j.ijheatmasstransfer.2018.05.087.

[8] A.A. Vasconcelos, A.O.C. Gomez, E.P.B. Filho, J.A.R. Parise, Experimental evaluation of SWCNT-water nanofluid as a secondary fluid in a refrigeration system, Appl. Therm. Eng. 111 (2017) 1487–1492, https://doi.org/10.1016/j.applthermaleng.2016.06.126.

[9] J. Zhou, X. Luo, Z. Feng, J. Xiao, J. Zhang, F. Guo, H. Li, Saturated flow boiling heat transfer investigation for nanofluid in minichannel, Exp. Therm Fluid Sci. 85 (2017) 189–200, https://doi.org/10.1016/j.expthermflusci.2017.03.002.

[10] R.L. Fragelli, L.E.A. Sanchez, R.R.I. Neto, V.L. Scalon, Refrigeration capacity of silver nanofluids under electrohydrodynamic effect oriented to heat removal in machining process, Exp. Therm Fluid Sci. 96 (2018) 11–19, https://doi.org/10.1016/j.expthermflusci.2018.02.022.

[11] A. Karimi, M. Afrand, Numerical study on thermal performance of an air-cooled heat exchanger: effects of hybrid nanofluid, pipe arrangement and cross section, Energy Convers. Manage. 164 (2018) 615–628, https://doi.org/10.1016/j.enconman.2018.03.038.

[12] M. Mehrali, E. Sadeghinezhad, R. Azizian, A.R. Akhiani, S.T. Latibari, M. Mehrali, H.S.C. Metselaar, Effect of nitrogen-doped graphene nanofluid on the thermal performance of the grooved copper heat pipe, Energy Convers. Manage. 118 (2016) 459–473, https://doi.org/10.1016/j.enconman.2016.04.028.

[13] Y. Zhou, X. Cui, J. Weng, S. Shi, H. Han, C. Chen, Experimental investigation of the heat transfer performance of an oscillating heat pipe with graphene nanofluids, Powder Technol. 332 (2018) 371–380, https://doi.org/10.1016/j.powtec.2018.02.048.

[14] M.A. Nazari, R. Ghasempour, M.H. Ahmadi, G. Heydarian, M.B. Shafii, Experimental investigation of graphene oxide nanofluid on heat transfer enhancement of pulsating heat pipe, Int. Commun. Heat Mass Transf. 91 (2018) 90–94, https://doi.org/10.1016/j.icheatmasstransfer.2017.12.006.

[15] Y. Yue, S.K. Mohammadian, Y. Zhang, Analysis of performances of a manifold microchannel heat sink with nanofluids, Int. J. Therm. Sci. 89 (2015) 305–313, https://doi.org/10.1016/j.ijthermalsci.2014.11.016.

[16] Q. Gravndyan, O.A. Akbari, D. Toghraie, A. Marzban, R. Mashayekhi, R. Karimi, F. Pourfattah, The effect of aspect ratios of rib on the heat transfer and laminar water/TiO_2 nanofluid flow in a two-dimensional rectangular microchannel, J. Mol. Liq. 236 (2017) 254–265, https://doi.org/10.1016/j.molliq.2017.04.030.

[17] M. Nojoomizadeh, A. Karimipour, M. Firouzi, M. Afrand, Investigation of permeability and porosity effects on the slip velocity and convection heat transfer rate of Fe_3O_4/water nanofluid flow in a microchannel while its lower half filled by a porous medium, Int. J. Heat Mass Transf. 119 (2018) 891–906, https://doi.org/10.1016/j.ijheatmasstransfer.2017.11.125.

[18] S. Chari, C. Kleinstreuer, Convective mass and heat transfer enhancement of nanofluid streams in bifurcating microchannels, Int. J. Heat Mass Transf. 125 (2018) 1212–1229, https://doi.org/10.1016/j.ijheatmasstransfer.2018.04.075.

[19] M. Kalteh, A. Abbassi, M. Saffar-avval, J. Harting, Eulerian – Eulerian two-phase numerical simulation of nanofluid laminar forced convection in a microchannel, Int. J. Heat Fluid Flow. 32 (2011) 107–116, https://doi.org/10.1016/j.ijheatfluidflow.2010.08.001.

[20] M. Kalteh, A. Abbassi, M. Saffar-avval, A. Frijns, A. Darhuber, Experimental and numerical investigation of nanofluid forced convection inside a wide microchannel heat sink, Appl. Therm. Eng. 36 (2012) 260–268, https://doi.org/10.1016/j.applthermaleng.2011.10.023.

[21] M. Mahdavi, M. Sharifpur, J.P. Meyer, CFD modelling of heat transfer and pressure drops for nanofluids through vertical tubes in laminar flow by Lagrangian and Eulerian approaches, Int. J. Heat Mass Transf. 88 (2015) 803–813, https://doi.org/10.1016/j.ijheatmasstransfer.2015.04.112.

[22] A. Esmaeilnejad, H. Aminfar, M. Sha, Numerical investigation of forced convection heat transfer through microchannels with non-Newtonian nanofluids, Int. J. Therm. Sci. 75 (2014) 76–86, https://doi.org/10.1016/j.ijthermalsci.2013.07.020.

[23] T. Ambreen, M.H. Kim, Comparative assessment of numerical models for nanofluids' laminar forced convection in micro and mini channels, Int. J. Heat Mass Transf. 115 (2017) 513–523, https://doi.org/10.1016/j.ijheatmasstransfer.2017.08.046.

[24] M.K. Moraveji, R.M. Ardehali, CFD modeling (comparing single and two-phase approaches) on thermal performance of Al_2O_3/water nanofluid in mini-channel heat sink ☆, Int. Commun. Heat Mass Transf. 44 (2013) 157–164, https://doi.org/10.1016/j.icheatmasstransfer.2013.02.012.

[25] W. Guo, G. Li, Y. Zheng, C. Dong, Numerical study of nanofluids thermal and hydraulic characteristics considering Brownian motion effect in micro fin heat sink, J. Mol. Liq. (2018) https://doi.org/10.1016/j.molliq.2018.04.152, #pagerange#.

[26] V. Kumar, J. Sarkar, Two-phase numerical simulation of hybrid nanofluid heat transfer in minichannel heat sink and experimental validation, Int. Commun. Heat Mass Transf. 91 (2018) 239–247, https://doi.org/10.1016/j.icheatmasstransfer.2017.12.019.

[27] C.J. Ho, C.Y. Chang, W.M. Yan, P. Amani, A combined numerical and experimental study on the forced convection of Al_2O_3-water nanofluid in a circular tube, Int. J. Heat Mass Transf. 120 (2018) 66–75, https://doi.org/10.1016/j.ijheatmasstransfer.2017.12.031.

[28] H. El Mghari, Experimental and numerical investigations of local condensation heat transfer in a single square microchannel under variable heat flux ☆, Int. Com-

mun. Heat Mass Transf. 71 (2016) 197–207, https://doi.org/10.1016/j.icheatmasstransfer.2015.12.021.
[29] H.A. Mohammed, G. Bhaskaran, N.H. Shuaib, H.I. Abu-mulaweh, Influence of nano fluids on parallel flow square microchannel heat exchanger performance ☆, Int. Commun. Heat Mass Transf. 38 (2011) 1–9, https://doi.org/10.1016/j.icheatmasstransfer.2010.09.007.
[30] T. Sheikhalipour, A. Abbassi, Numerical analysis of nanofluid flow inside a trapezoidal microchannel using different approaches, Adv. Powder Technol. (2018) https://doi.org/10.1016/j.apt.2018.04.010.
[31] A.A. Alfaryjat, H.A. Mohammed, N. Mariah, D. Stanciu, A. Dobrovicescu, Numerical investigation of heat transfer enhancement using various nano fl uids in hexagonal microchannel heat sink, Therm. Sci. Eng. Prog. 5 (2018) 252–262, https://doi.org/10.1016/j.tsep.2017.12.003.
[32] T. Bello-Ochende, O.O. Adewumi, J.P. Meyer, Increased heat load effects on the thermal performance of single- and two-layered microchannels with varying axial length and micro pin-fin inserts, Int. J. Fluid Mech. Res. 43 (2016) https://doi.org/10.1615/InterJFluidMechRes.v43.i56.60.
[33] O.O. Adewumi, T. Bello-Ochende, J.P. Meyer, Numerical investigation into the thermal performance of single microchannels with varying axial length and different shapes of micro pin-fin inserts, Heat Transf. Eng. 38 (2017) 1157–1170, https://doi.org/10.1080/01457632.2016.1239927.
[34] F. Hong, P. Cheng, Three dimensional numerical analyses and optimization of offset strip- fin microchannel heat sinks, Int. Commun. Heat Mass Transf. 36 (2009) 651–656, https://doi.org/10.1016/j.icheatmasstransfer.2009.02.015.
[35] A. Shahsavar, M. Moradi, M. Bahiraei, Heat transfer and entropy generation optimization for flow of a non-Newtonian hybrid nanofluid containing coated CNT/Fe_3O_4 nanoparticles in a concentric annulus, J. Taiwan Inst. Chem. Eng. 84 (2018) 28–40, https://doi.org/10.1016/j.jtice.2017.12.029.
[36] M. Hojjat, S.G. Etemad, R. Bagheri, J. Thibault, Rheological characterisitcs of non-Newtonian nanofluids: experimental investigation, Int. Commun. Heat Mass Transfer 38 (2011) 144–148, https://doi.org/10.1016/j.icheatmasstransfer.2010.11.019.
[37] M. Hojjat, S.G. Etemad, R. Bagheri, J. Thibault, Thermal conductivity of non-Newtonian nanofluids: experimental data and modeling using neural network, Int. J. Heat Mass Trasnfer 54 (2011) 1017–1023, https://doi.org/10.1016/j.ijheatmasstransfer.2010.11.039.
[38] M. Hojjat, S.G. Etemad, R. Bagheri, J. Thibault, Turbulent forced convection heat transfer of non-Newtonian nanofluids, Exp. Therm. Fluid Sci. 35 (2011) 1351–1356, https://doi.org/10.1016/j.expthermflusci.2011.05.003.
[39] S. Baheri Islami, B. Dastvareh, R. Gharraei, An investigation on the hydrodynamic and heat transfer of nanofluid flow, with non-Newtonian base fluid, in micromixers, Int. J. Heat Mass Transf. 78 (2014) 917–929, https://doi.org/10.1016/j.ijheatmasstransfer.2014.07.022.
[40] M. Bahiraei, M. Alighardashi, Investigating non-Newtonian nanofluid flow in a narrow annulus based on second law of thermodynamics, J. Mol. Liq. 219 (2016) 117–127, https://doi.org/10.1016/j.molliq.2016.03.007.
[41] M. Bahiraei, S. Heshmatian, Application of a novel biological nanofluid in a liquid block heat sink for cooling of an electronic processor: thermal performance and irreversibility considerations, Energy Convers. Manage. 149 (2017) 155–167, https://doi.org/10.1016/j.enconman.2017.07.020.
[42] M. Khoshvaght-Aliabadi, F. Hormozi, A. Zamzamian, Experimental analysis of thermal–hydraulic performance ofcopper-water nanofluid flow in different plate-fin channels, Exp. Therm Fluid Sci. 52 (2014) 248–258, doi: 10.1016/j.expthermflusci.2013.09.018.
[43] J.H. Lienhard, J.H. Lienhard, A Heat Transfer Textbook, second ed., Phlogiston Press, 2002.